

## MODAL NOISE MITIGATION THROUGH FIBER AGITATION FOR FIBER-FED RADIAL VELOCITY SPECTROGRAPHS

RYAN PETERSBURG, TYLER MCCRACKEN, DOMINIC EGGERMAN, COLBY JURGENSON, DAVID SAWYER, DEBRA FISCHER  
Department of Astronomy, Yale University, 52 Hillhouse Ave, New Haven, CT 06511, USA; ryan.petersburg@yale.edu

*Draft version August 2, 2017*

### ABSTRACT

Optical fiber modal noise is a critically limiting factor for high precision spectroscopy signal-to-noise in the near-infrared and visible. Unabated, especially for highly coherent light sources, modal noise can induce radial velocity errors that hinder the discovery of low-mass (and potentially earth-like) planets. Previous research in this field has found sufficient modal noise mitigation through use of an integrating sphere, but this requires extremely bright light sources, a luxury not necessarily afforded calibration for the next-generation of high resolution optical-range spectrographs. Otherwise, mechanical agitation, which “mixes” the fiber’s modal patterns and allows the noise to be averaged over minutes-long exposures, provides some noise reduction but the methods have not been fully optimized by the community. Therefore, we have filled out the parameter space of modal noise agitation techniques in order to better understand agitation’s contribution to mitigating modal noise and to discover the optimal strategy for agitating fibers. We found that modal noise was best suppressed by the chaotic nature of coupled harmonic motion at high amplitude for fibers with large core diameters and low azimuthal symmetry, reducing modal noise induced radial velocity error to below 10 cm/s. This work has subsequently influenced the design of a fiber agitator to be installed with the Extreme Precision Spectrograph.

### 1. INTRODUCTION

Radial velocity (RV) exoplanet detection has continually been on the path of discovering less massive planets. The current goal of RV spectroscopy is 10 cm s<sup>-1</sup> precision, thereby allowing the discovery of earth-like planets orbiting G and K stars in their respective habitable zone (Fischer et al. 2016). Therefore, the next-generation of visible-band RV spectrographs, such as the Extreme Precision Spectrograph (EXPRES, Jurgenson et al. 2016) and ESPRESSO Mégevand et al. (2012), require precision engineering and extreme stability to yield such results.

 Multi-mode fibers have become the backbone of such RV spectrograph design. An essential link between the telescope focus and the spectrograph optics, optical fibers isolate the spectrograph from vibrational and thermal noise. Optical fibers also provide spatial scrambling to stellar light since the spatial distribution of a fiber output is, for the most part, independent of the input (Hunter & Ramsey 1992). This effect has been amplified through the use of double scramblers (Halverson et al. 2015a; Spronck et al. 2015) and non-circular fiber core cross-sectional shapes including octagons and rectangles (Chazelas et al. 2010; Spronck et al. 2012; Plavchan et al. 2013).

Optical fibers also transmit light from calibration sources—such as wavelength calibrators and broadband flat-field sources—into the spectrograph. Laser frequency combs, especially the astrocomb (Probst et al. 2014) recently deployed at HARPS and soon to be with EXPRES, produce thousands of evenly spaced high-finesse emission lines over a wide frequency range. When these highly coherent lines propagate through a multi-mode fiber, they create a source of noise that limits the signal-to-noise ratio (SNR) of the instrument and potentially induces false signals into the data. This noise is caused

by interference between the finite number of electromagnetic modes that can propagate along a multi-mode fiber, 

 Some next-generation RV spectrographs (e.g. iLocater, Crepp et al. 2016) have moved to a completely single-mode fiber architecture to help alleviate these complications. As apparent in their name, single-mode fibers only propagate a single electromagnetic mode and are therefore free from any modal noise. Due to the small core-size of single-mode fibers, however, coupling light from the telescope into these fibers is challenging, requiring robust adaptive optics that have not yet been fully developed. Additionally, single-mode fibers have a very limited bandwidth over which they propagate a single-mode. Therefore, these fibers may not be truly single-mode across the full band of wavelength calibration meaning the optical design requires multiple band-depend paths. Finally, Halverson et al. (2015b) asserts that a type of polarization “modal noise” exists in single mode fibers. Thus, the study of modal noise reduction methods may still be necessary even for these novel single-mode-fiber injected instruments.

 In this paper, we attempt to discern the optimal strategy for reducing modal noise in multi-mode fibers propagating coherent visible light through mechanical agitation. We begin by defining modal noise and exploring how previous experiments have mitigated it through static and dynamic methods (section 2). We then describe our own methods of fiber agitation (section 3) and discuss results from using these methods on fibers of varying cross-sectional shapes and coupling permutations (section 4). Finally, we relate these results to limits in RV precision (section 5) and discuss how these results should be applied to next-generation RV spectrographs (section 6). The work in this paper was conducted to influence design decisions for EXPRES.

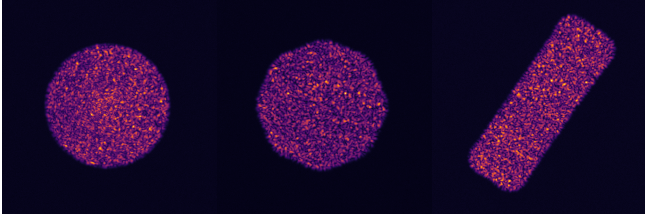


FIG. 1.— Examples of unmitigated modal noise for a rectangular (left), octagonal (middle), and circular (right) optical fiber. All three fibers shown here have approximately the same cross-sectional area, meaning that they each are propagating about the same number of electromagnetic modes (see section 3). Brightness in this image is scaled by the square root of photon count to emphasize the speckles.

## 2. OPTICAL FIBER MODAL NOISE

Light propagates through an optical fiber in an integer number of electromagnetic modes. The exact calculation for this value is non-trivial since it depends on the instantaneous fiber geometry, injection parameters, and many other variables. The maximum number of modes for a step-index circular cross-section fiber is approximately given by

$$M_{circ} \approx \frac{4}{\pi^2} V^2 \quad (1)$$

where  $V$  is the normalized frequency of the fiber given as

$$V = \left( \frac{2\pi r \text{NA}}{\lambda} \right)^2. \quad (2)$$

$\text{NA} = \sqrt{n_{core}^2 - n_{clad}^2}$  is the numerical aperture of the fiber determined by the core ( $n_{core}$ ) and cladding ( $n_{clad}$ ) indices of refraction,  $r$  is the core radius, and  $\lambda$  is the wavelength of propagated light. This approximation is more difficult for a rectangular fiber, but Nikitin et al. (2011) shows empirically using electromagnetic and geometrical arguments that

$$\frac{M_{rect}}{M_{circ}} \propto \frac{ab}{r^2} \quad (3)$$

where  $a$  and  $b$  are the side lengths of the rectangular cross-section. Therefore, we will assert more generally that

$$M \propto A \left( \frac{\text{NA}}{\lambda} \right)^2 \quad (4)$$

where  $A$  is the cross-sectional area of the fiber regardless of shape.

When coherent light is propagated through a multi-mode fiber, a high contrast speckle pattern known as modal noise is produced at the output for both the near-field (fiber face) and far-field, figure 1. Modal noise is an inherent property of all multi-mode fibers regardless of the cross-sectional core shape (Sablowski et al. 2015) and arises from light coupling from mode-to-mode as it propagates through fiber, causing slight variances in the path length traveled and producing the observed interference pattern. For RV spectrographs this causes two problems: 1) it limits the maximum signal-to-noise ratio and 2) systematic variations in the speckle pattern will mask themselves as minute shifts on the focal plane causing errant RV signatures.

### 2.1. Limit on SNR

Due to its high contrast, modal noise can severely decrease the signal-to-noise ratio of an RV spectrograph (Epworth 1978; Baudrand & Walker 2001; Lemke et al. 2011). Additionally, if the speckle pattern drifts between exposures, especially with some period of motion, modal noise can cause errant RV signatures in the data that is distinct from errors due to poor scrambling (Mahadevan et al. 2014).

Modal noise's dependence on static physical properties of optical fibers is well documented and follows from theory. Modal noise SNR is increased for larger fiber core diameters as in equation 1 (Sablowski et al. 2015; Lemke et al. 2010) and for non-circular fibers over circular fibers (Stürmer et al. 2016; Sablowski et al. 2015). Increasing the number of static bends in a fiber slightly increases SNR (Imai & Asakura 1979). Far field modal noise SNR is strongly anti-correlated with injected focal ratio (Sablowski et al. 2015), while the near field modal noise SNR is independent of injected focal ratio (Baudrand & Walker 2001). Finally, modal noise SNR was shown to be anti-correlated with wavelength (as expected by equation 1), poorly responsive to input pupil obstructions, and independent of fiber length greater than a few meters (Baudrand & Walker 2001).

### 2.2. Dynamic variations

Modal noise is also affected by dynamic optical properties, meaning it can induce false RV's on the spectrograph, in addition to being an issue of SNR. The speckle pattern is heavily wavelength dependent as seen in equation 4. However, next-generation RV spectrographs are using stable wavelength calibrators rendering this problem effectively irrelevant. Otherwise, the speckle pattern seen at the end of a fiber shifts over time due to many reasons, but most commonly because of (Epworth 1978):

1. Temperature variation
2. Fiber input illumination variation
3. Fiber movement (bending, twisting, etc.)

These three conditions inevitably pose problems when imaging a spectrum since they are inherent to modern fiber-fed RV spectrographs (Baudrand & Walker 2001; Mahadevan et al. 2014). There is typically a temperature difference between the telescope and the spectrograph, fluctuations in atmospheric density change the fiber illumination, and the telescope slowly slews throughout the night.

Modal noise can be reduced by continuously exacerbating one of the above three causes of drift, thereby shifting the speckle pattern throughout an appropriately long camera exposure and averaging out the noise. Controlled temperature variation (option 1) is non-ideal because a 1 meter fiber requires approximately  $8^\circ\text{C}$  fluctuations to visibly decorrelate the speckle pattern (Redding et al. 2013), a temperature change much too large to guarantee optomechanical stability. Therefore, RV spectrographs have been left with either varying the illumination (option 2) or shaking the fiber (option 3).

As summarized in table 1, modal noise reduction techniques have been discussed by many experiments concerned with RV spectroscopy. The majority deal with



TABLE 1  
PREVIOUS STUDY OF DYNAMIC MODAL NOISE MITIGATION METHODS

Reference	Method	Frequency	Amplitude
Daino et al. (1980)	Loudspeaker	110 Hz	“Sufficient”
Baudrand & Walker (2001)	—	30 Hz	1 mm
Lemke et al. (2011)	Loudspeaker	1.5 Hz	—
	Loudspeaker	80 Hz	—
	Paint mixer	60 Hz	—
McCoy et al. (2012)	Hand agitated	1-2 Hz	10-15 cm
	Mechanical agitator	“Low”	“High”
Plavchan et al. (2013)	“Tweeter”	100 Hz	1 mm
	“Woofer”	1 Hz	25 mm
Mahadevan et al. (2014)	Int. Sph. + Diff.	—	—
	McCoy agitator	“Low”	“High”
	Hand agitation	1-2 Hz	10 cm
Halverson et al. (2014)	Int. Sph. + Diff.	—	—
	Int. Sph. + OAP	—	—
Roy et al. (2014)	Rail agitator	“Low”	“High”
Sablowski et al. (2015)	Mechanical “Excenter”	2 Hz	20 cm

some form of agitation that physically changes the position of the fiber (mechanical agitation) while Mahadevan et al. (2014) and Halverson et al. (2014) explored the effectiveness of varying the illumination of the fiber face. The variation in frequency and amplitude for the mechanical agitation methods is unfortunately quite wide and connections are difficult to make. However, there have been slight trends in the results and the discussed assumptions so far are as follows:

- The frequency of agitation should be greater than  $1/\tau$ , where  $\tau$  is the exposure time (Baudrand & Walker 2001)
- Noise is more effectively reduced by high amplitude motion (Lemke et al. 2011; McCoy et al. 2012)
- Higher frequencies (with an upper limit) show further noise reduction (Lemke et al. 2011)
- Adding a high frequency “tweeter” to a large amplitude “woofer” reduces noise further (Plavchan et al. 2013)
- Hand agitation is better than any form of mechanical agitation (Lemke et al. 2011; McCoy et al. 2012; Mahadevan et al. 2014; Roy et al. 2014)

Although this has been good for subjective intuition, the exact mechanisms behind the improvements in SNR and prevention of RV drift have not been explored.

Varying the input illumination of a fiber using an integrating sphere, diffuser, and rotating mirror showed gradual improvements in modal noise reduction due to the addition of further illumination variation. However, the integrating sphere, an integral part of these methods, has a throughput efficiency of approximately  $10^{-6}$  and is not feasible to be introduced in the science light optical path. To allow flexible observing programs, i  science observations bracketed by precision wavelength calibration sources, the modal noise mitigation technique needs to be efficient.

In the following sections, we fill out the parameter space of fiber agitation methods to a greater extent than previous studies. We are interested in seeing trends across different amplitudes, frequencies, fiber shapes/sizes, and coupling permutations to make more precise conclusions about the nature of modal noise mitigation through fiber agitation.

TABLE 2  
TESTED OPTICAL FIBERS. ALL FIBERS HAVE NA = 0.22.

Shape	Size	Manufacturer
Circular	100 µm	Polymicro
Circular	200 µm	Polymicro
Circular	600 µm	Thorlabs
Octagonal	100 µm	CeramOptec
Octagonal	200 µm	CeramOptec
Rectangular	100 µm × 300 µm	CeramOptec

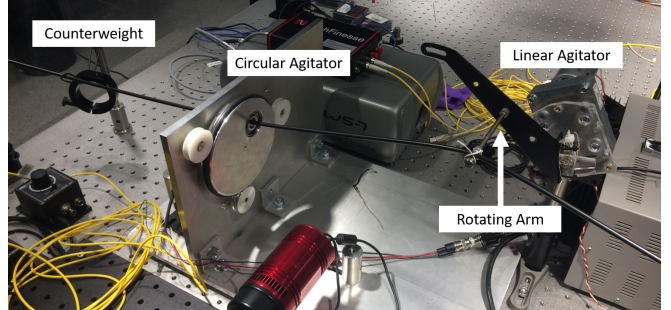


FIG. 2.— Linear and circular agitator used in these modal noise tests. The linear agitator rotates along the length of the fiber while the circular agitator rotates perpendicular to it. A small counterweight is present to keep a minimal amount of tension in the fiber and prevent it from over-bending or bunching up.

### 3. EXPERIMENTAL SETUP

The number of modes a fiber supports is largely determined by its cross-sectional area. For testing and characterizing agitation methods across multiple fiber geometries, we chose a fibers with similar cross-sectional areas. Table 2 lists the fibers used in our experiment. Notice that the 200 µm circular, 200 µm octagonal, and 100 µm × 300 µm rectangular fiber all have approximately the same cross-sectional area, meaning they can each support a similar number of modes.

Two different methods of mechanical agitation are used: the first produces a linear type motion in which the fiber is moved up and down, the other is a circular type motion in which the fiber cross section is rotated perpendicular to direction of propagation. The linear agitation has variable amplitude allowing for 80-320 mm agitation amplitudes at 80 mm intervals and a variable frequency in the range of 0.03 to 1.0 Hz. For the circular agitator, the fiber is rotated in circular path with a set amplitude of 80 mm at a variable frequency of 0.1 to



FIG. 3.— PASCO Scientific economy wave driver used to test high-frequency, low-amplitude agitation (tweeter). [https://www.pasco.com/images/products/wa/WA9854\\_MAIN\\_171382.jpg](https://www.pasco.com/images/products/wa/WA9854_MAIN_171382.jpg)

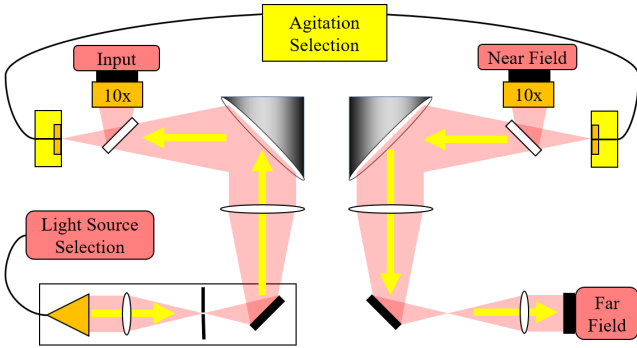


FIG. 4.— Schematic of the Fiber Characterization Station. Light from either a single-mode fiber-fed 652 nm Toptica diode laser or from a selection of Thorlabs mounted LEDs fed by a 100  $\mu\text{m}$  circular fiber is fed into the station in the bottom left. This light is spatially filtered, collimated, and injected into the test fiber. The injection face of the test fiber is imaged at 10x magnification by the input camera to allow for precision alignment. Light propagates through the test fiber and our choice of agitator mixes the modes. Light is then ejected from the test fiber and split between the 10x magnified near field camera and the far field camera.

TABLE 3  
FIBER CHARACTERIZATION STATION IMAGING SPECIFICATIONS

Name	Camera	Pixel Size	Magnification
Input	Atik 450	3.45 $\mu\text{m}$	10
Near Field	Atik 450	3.45 $\mu\text{m}$	10
Far Field	Atik 383L+	5.4 $\mu\text{m}$	N/A

1.5 Hz. Routing a fiber through both agitators produces what we call “coupled agitation”. Both agitators are shown in figure 2, frequencies are independently set by adjusting the appropriate DC-motor drive voltage. The amplitude of the linear agitator is set by the position of the lifting arm and a small counterweight is present to keep a minimal amount of tension in the fiber between the agitators and prevent it from folding on itself.

To test high-frequency, low-amplitude agitation, we use a PASCO Scientific “Economy Wave Driver” shown in figure 3. This device, attached to a sine wave function generator, produces approximately 5 mm amplitude for 10-30 Hz oscillations. It can be driven at higher frequencies, but the amplitude would not be large enough to produce significant fiber motion.

All image data was collected with the Fiber Characterization Station (FCS, figure 4), a multipurpose device that is able to simultaneously image the input face, output face (or near field), and output pupil (or far field) of the fiber under test. Specifications for the FCS cameras are listed in table 3.

Images exposure times are set according to the fre-

quency of agitation such that each exposure lasts exactly one period of rotation. For example, if an agitator is set to rotate at 0.5 Hz, each image will be exposed for 2 s. We do this to confirm that only one full rotation is being recorded and allow for “number of rotations” to be another parameter for exploration.

Each data set is comprised of a 10 exposures each of the following cases:

1. the fiber being actively agitated
2. the fiber routed through the agitator but without agitation
3. the unagitated fiber illuminated with a broadband LED.

Multiple images are taken to reduce statistical errors in our SNR calculations potentially caused by camera noise or small problems with our agitators and to observe the effects of agitation at longer exposures time by co-adding multiple single-rotation images together. The LED source acts as a best-case scenario and the unagitated as a worst case.

We quantify modal noise using the SNR of light within the fiber face of the near field image calculated as

$$\text{SNR} = \frac{\text{median}(I_{filt})}{\text{stdev}(I_0 - I_{filt})} \quad (5)$$

where  $I_0$ , the original raw image, is heavily median filtered to produce  $I_{filt}$ . The typical SNR (where the “signal” is assumed to be a top-hat function across the fiber face) could not be used due to slight intensity-varying diffraction effects across the near field image. Subtracting  $I_{filt}$  from  $I_0$  therefore produces a noise pattern that reflects the modal noise and not these large-scale diffraction-caused variances. We use a circular 51-pixel median filter rather than a low-order polynomial or Gaussian fit because these functions could not sufficiently fit the raw fiber images. The size of the filter kernel was chosen such that speckles on unagitated images were sufficiently filtered without removing structure from the edges of the fibers. The numerator in equation 5 is calculated as the median (rather than the mean, for example) of  $I_{filt}$  to prevent dust on the fiber face or optics from skewing this value.

We calculate the SNR for each individual image and average them together within each data set to yield a single-rotation SNR. We then co-add images 1-2, 1-3, 1-4, ..., 1-10 and calculate the SNR for each case. The SNR for images 1-10 is presented as the ten-rotation SNR and each intermediate step as two-rotation SNR, three-rotation SNR, etc.

Far field images are taken for each data set and analyzed using the maximum intensity rather than the median intensity as the numerator in equation 5. The far field speckle pattern is of interest in precision RV spectroscopy as it is what illuminates the optics. However, mapping the far field speckle pattern to RV error would require numerical simulations with the optical design software and is out of the scope of this paper. That being said, all results listed in the following section may be extended to the far field though we omit this data for conciseness.

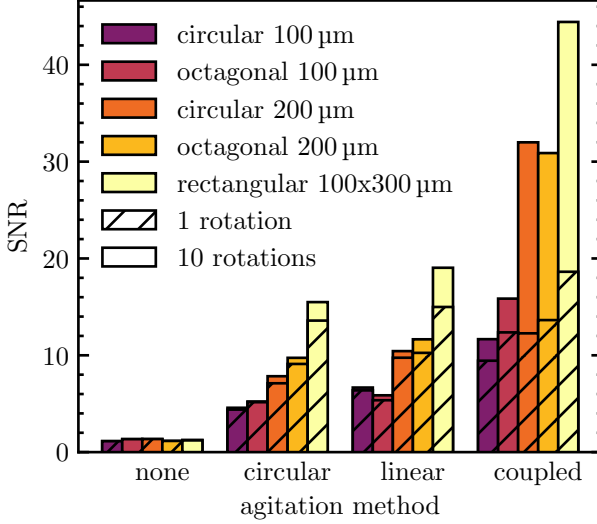


FIG. 5.— SNR comparison for varying fiber geometries and agitation methods. SNR for 10 rotation images was calculated after co-adding ten single rotation images.

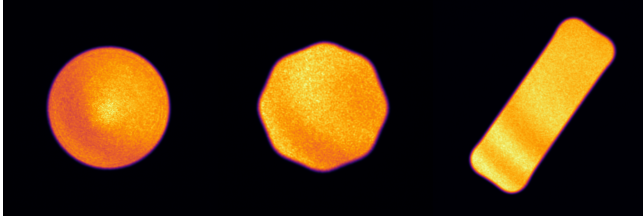


FIG. 6.— Ten-rotation, coupled agitation images using the same three fibers shown in figure 1. The diffraction pattern is clearly seen, but otherwise, the presence of speckles in these images is significantly diminished. With larger amplitude in both the circular and linear agitator, the SNR will continue to improve. These images were taken as part of the data in section 4.1.

#### 4. RESULTS

##### 4.1. Method of Agitation and Fiber Geometry

We compare the two individual agitation methods and coupled agitation using all of the fibers previously listed in table 2. The linear agitator was set to an amplitude of 80 mm and the frequency of both agitators to 1.0 Hz, all images are taken with 1 s exposures.

Results for the single-rotation and ten-rotation cases are shown in figure 5. Across all fiber shapes and sizes and number of rotations, the linear agitator appears to be slightly better than the circular agitator. There is a similar increase in SNR when looking at coupled agitation in single-rotations. However, coupling the agitation over ten-rotations significantly increases the SNR for all fiber configurations.

Ten-rotation images of the three larger fibers using the coupled agitation method are shown in figure 6. Compared to those shown in figure 1, the speckle patterns when using coupled agitation are nearly non-existent.

To better understand why coupled agitation is so effective at reducing modal noise at longer exposures, we also analyze the effect of each agitation method over multiple rotations, as shown in figure 7 for the 100 μm × 300 μm rectangular fiber. SNR shows continued improvement beyond a single rotation when coupling the agitation

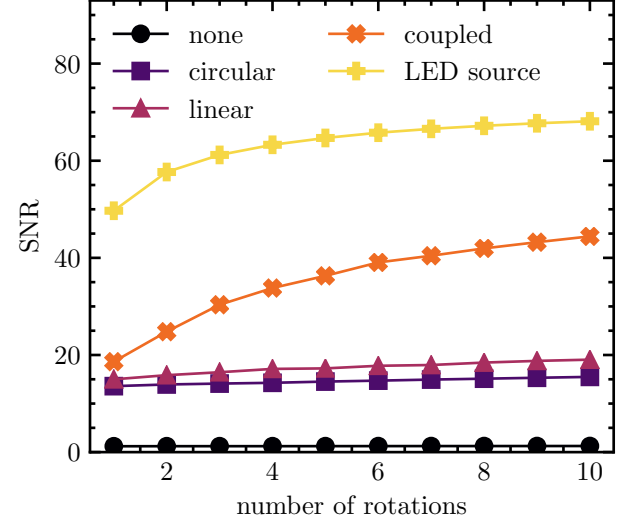


FIG. 7.— SNR for the 100x300 μm rectangular fiber using various agitation methods. The SNR is calculated after co-adding the 1 rotation images.

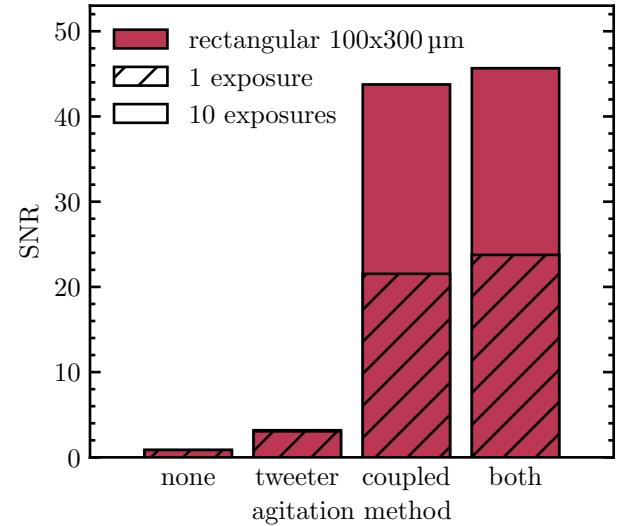


FIG. 8.— SNR comparison when adding a tweeter to the coupled agitation method for a rectangular fiber. Exposure times are set to 2.0 s, approximately the period of one rotation for the coupled agitator, and the tweeter is set to 20 Hz.

methods at a similar rate to when the fiber is lit by an LED, a broadband source. Circular and linear agitation, however, are effectively plateaued after the first rotation.

##### 4.2. Adding a Tweeter

We also test the high-frequency, low-amplitude tweeter proposed by (Plavchan et al. 2013) in tandem with our coupled agitation to see if it supplies significant improvement to modal noise SNR. We set the linear agitator to 240 mm and 0.5 Hz and the circular agitator to approximately the same frequency. All exposure times are set to 2.0 s.

The results are shown in figure 8. The tweeter improves SNR above coupled agitation alone regardless of exposure time. However, the magnitude of this improvement

TABLE 4  
FIBER ASSEMBLIES TESTED FOR THE FIBER COUPLING EXPERIMENT

Test	1st Fiber	2nd Fiber
1	Circular 200 $\mu\text{m}$	Circular 200 $\mu\text{m}$
2	Circular 100 $\mu\text{m}$	Circular 200 $\mu\text{m}$
3	Octagonal 200 $\mu\text{m}$	Circular 200 $\mu\text{m}$

is minimal and is far outweighed by the improvement due to coupled agitation.

#### 4.3. Amplitude and Frequency of Agitation

We use the  $100 \mu\text{m} \times 300 \mu\text{m}$  rectangular fiber and the two agitators separately to test the effects of agitation amplitude and frequency of rotation on the SNR. We can only test amplitude on the linear agitator and take an image set for each position on the rotating arms. We test frequency on each of the linear and circular agitators at approximately equally spaced frequencies across their entire frequency range.

Results from these tests are shown in figure 9. There is a strong position correlation between linear agitation amplitude using both the single-rotation and ten-rotation analyses. There also appears to be a slight increase in SNR for the linear agitator at higher frequencies after ten rotations, however there is no such increase for the single-rotations or any of the frequencies when using the circular agitator.

#### 4.4. Fiber Coupling

It is not uncommon for RV spectrographs to have multiple fiber links for carrying calibration and/or science light from the source (lamp or telescope respectively) to the spectrograph and ultimately detector. This results in having to couple light from one fiber to another and begs the question, is there a preferred fiber to agitate or must we agitate as many as possible? Agitating the first fiber in a multi-fiber system serves to vary the input illumination of subsequent fibers, similar to the integrating sphere proposed by (Mahadevan et al. 2014) and (Halverson et al. 2014). To study the effects of such an architecture, we agitated individual fibers in a multi-fiber assembly where each fiber could have different core sizes and shape. We test three distinct cases outlined in table 4 and compare them against agitating a single  $200 \mu\text{m}$  circular fiber. For this test fibers were agitated using the linear agitator at 80 mm and 1.0 Hz.

The results from these tests are shown in figure 10. For the most part, the SNR for each test hovers around 10, the same level at which the SNR would be for an uncoupled  $200 \mu\text{m}$  fiber. However, the SNR when agitating only the  $100 \mu\text{m}$  fiber is significantly less than 10. The single-rotation images when agitating the second fiber in the  $200\text{-}200 \mu\text{m}$  test also seem to be abnormally low, but this appears to be repaired over longer exposures. Otherwise, the SNR when agitating both the coupled  $200 \mu\text{m}$  octagonal and  $200 \mu\text{m}$  circular fibers simultaneously is significantly improved.

#### 4.5. Discussion

Our results can be summarized as follows, the highest SNR is attained when a fiber has been put through as many physical configurations as possible over the length of an exposure. This is best accomplished using a coupled agitation setup comprised of, in our case, a linear

and circular motion with the highest amplitude possible on each. One could conceive a random or chaotic agitator as a possible implementation. These conclusions are highly reminiscent of the idea that hand-agitation is consistently better than any form of mechanical agitation. Human motions are much less deterministic than a motor resulting in a more chaotic motion. Our combined linear/circular agitator with slightly different oscillation frequency mimics this behavior since it will chaotically reach many fiber configurations over a single calibration exposure of about 10 s. Note that the motion needs to be continuous to avoid build-up of a static speckle pattern within the exposure.

Our results indicate that large amplitude, relatively high frequency, chaotic coupled harmonic agitation for optical fibers that have large core cross-sectional area and low azimuthal symmetry yield the highest signal to noise. We therefore believe that the most important factor when agitating fibers is to place the fiber into as many physical configurations as possible over a single exposure, and can be done anywhere along the length of the fiber, allowing for large distance from a stabilized spectrograph.

We made this conclusion initially from the data present in figure 9 which shows a much stronger correlation between amplitude and SNR than between frequency and SNR. The data in figures 5 and 7 provide further evidence that placing the fiber into more physical configurations further increases the SNR.

Our tweeter tests also provide evidence for our conclusion. Even though the high-frequency device is able to place the fiber into many positions over a single exposure, the difference in these configurations is relatively small. Therefore, the speckle pattern is only “fuzzed” a little rather than moved throughout the entire fiber face. Adding a tweeter to a large-amplitude agitator does show some small improvements (since extra “fuzzing” would naturally increase SNR), but these improvements are significantly overshadowed by simply having large amplitude motion.

We are also able to confirm previous results that show better mitigation of modal noise for fibers with larger cross-sectional areas and less azimuthally symmetry. As seen in figure 5, across all agitation methods, the  $200 \mu\text{m}$  fibers fared better than the  $100 \mu\text{m}$  fibers and the rectangular fiber was consistently far better than the others.

It follows that the location of agitation in a fiber architecture should depend primarily on the cross-sectional area of the fiber. Figure 10 shows that SNR is only significantly worsened if the smaller fiber in a system is agitated over the larger one. This is consistent with our previous conclusion that smaller fibers are less effective when mitigating modal noise. Otherwise, our results indicate that agitating more fibers is helpful, especially if they have different core shapes, but not significantly enough to warrant necessitating this in the design.

Moreover, location of agitation along a single fiber does not seem to matter. Coupling two  $200 \mu\text{m}$  fibers with a 1:1 ratio is effectively adding their lengths together. As shown by figure 10, the location of agitation is irrelevant, especially for ten-rotation exposures. Therefore, the agitator could be placed anywhere along the length of the fiber (preferably far away from the spectrograph) and it will produce the same magnitude effect on modal noise.

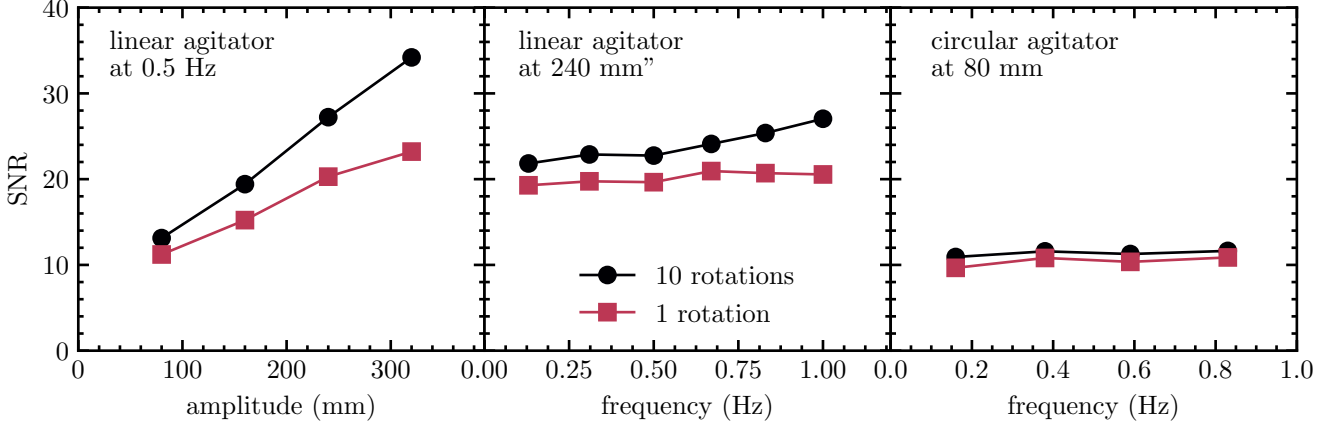


FIG. 9.— SNR comparison for varying amplitudes using the linear agitator (left) and varying frequencies using each of the linear (center) and circular (right) agitators. For the amplitude tests, the linear agitator was set at 0.5 Hz. For the linear agitator frequency test, the amplitude was set to 240 mm. The circular agitator can only be set to an amplitude of 80 mm. Integration times were set to match the period of 1 rotation (i.e. 2 s for 0.5 Hz agitation). The “10 rotations” data was calculated after co-adding 10 of these 1 rotation images. Results in the far field yielded similar correlations between amplitude, frequency, and SNR.

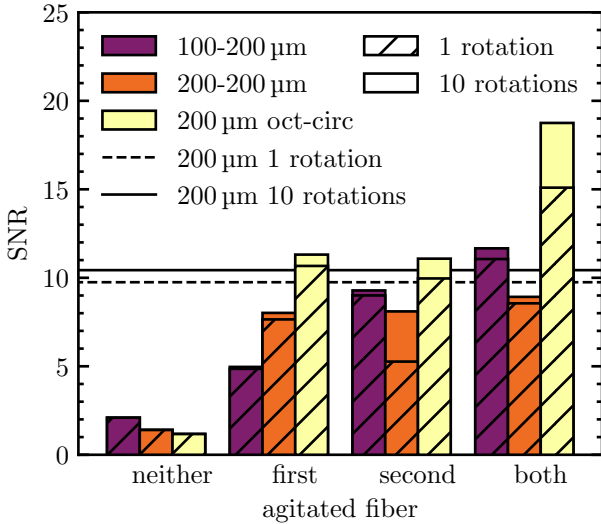


FIG. 10.— SNR for various arrangements of coupled fibers with varying core diameter and cross-sectional shape. All fibers are assumed to be circular unless otherwise stated on the plot. The SNR for a single 200 μm circular fiber is also presented for both 1 rotation (dashed) and 10 rotations (solid).

This conclusion relies on only one test, however, so it will require further study to absolutely confirm.

##### 5. RADIAL VELOCITY PRECISION

As discussed in section 2, optical fiber modal noise is an issue of centroid drift as well as diminished SNR. To observe how the centroid actually drifts over time, we test our agitation method on the 100 μm × 300 μm rectangular fiber over three hundred 1.0 s exposures.

The resultant RV precision ( $\sigma_{RV}$ ) due to a shifting speckle pattern centroid at the end of a fiber is calculated as:

$$\sigma_{RV} \approx \frac{c \sigma_d}{R D} \quad (6)$$

where  $c$  is the speed of light in a vacuum,  $R$  is the resolution of the spectrograph,  $\sigma_d$  is the standard deviation of

fiber near field centroid drift in the dispersion direction and  $D$  is the slit width (or short-end length of a rectangular fiber). Importantly,  $\sigma_{RV}$  is only the RV error *per resolution element* or *per line* from a wavelength calibration source. Averaging over  $N$  lines, we can divide  $\sigma_{RV}$  by  $\sqrt{N}$  to get the total RV error. Notice that for a  $R = 150,000$  spectrograph fed by a 33 μm slit attempting to reach  $1 \text{ m s}^{-1}$  RV precision per line, the required stability of the centroid along the dispersion direction is 0.0165 μm.

We derive equation 6 from the low velocity approximation of the relativistic Doppler effect

$$\frac{\Delta\lambda}{\lambda} = \sqrt{\frac{1+v/c}{1-v/c}} - 1 \approx \frac{v}{c} \quad (7)$$

where  $\Delta\lambda$  is the measured shift in wavelength at wavelength  $\lambda$  on the spectrograph for a star moving at velocity  $v$  relative to Earth. We also define the resolution of the spectrograph

$$R = \frac{\lambda}{\Delta\lambda_R} \quad (8)$$

where  $\Delta\lambda_R$  is the width of the spectrograph resolution element in terms of wavelength bandwidth. Finally, we know the relationship between a fiber near field centroid shift and a measured wavelength shift on the spectrograph:

$$\frac{\Delta d}{D} = \frac{\Delta\lambda}{\Delta\lambda_R}. \quad (9)$$

Using equations 7, 8, and 9 we show that

$$\frac{v}{c} \approx \frac{\Delta\lambda}{\lambda} = \frac{1}{R} \frac{\Delta\lambda}{\Delta\lambda_R} = \frac{1}{R} \frac{\Delta d}{D}. \quad (10)$$

If we take the standard deviation of the data from each side of this equation ( $v \rightarrow \sigma_{RV}$ ,  $\Delta d \rightarrow \sigma_d$ ) and move  $c$  to the right side, we get equation 6.

The idealized agitation method we use to test RV precision includes the circular agitator oscillating at 1.1 Hz and the linear agitation set at 240 mm and 1.0 Hz. Keeping the two agitators at slightly different frequencies

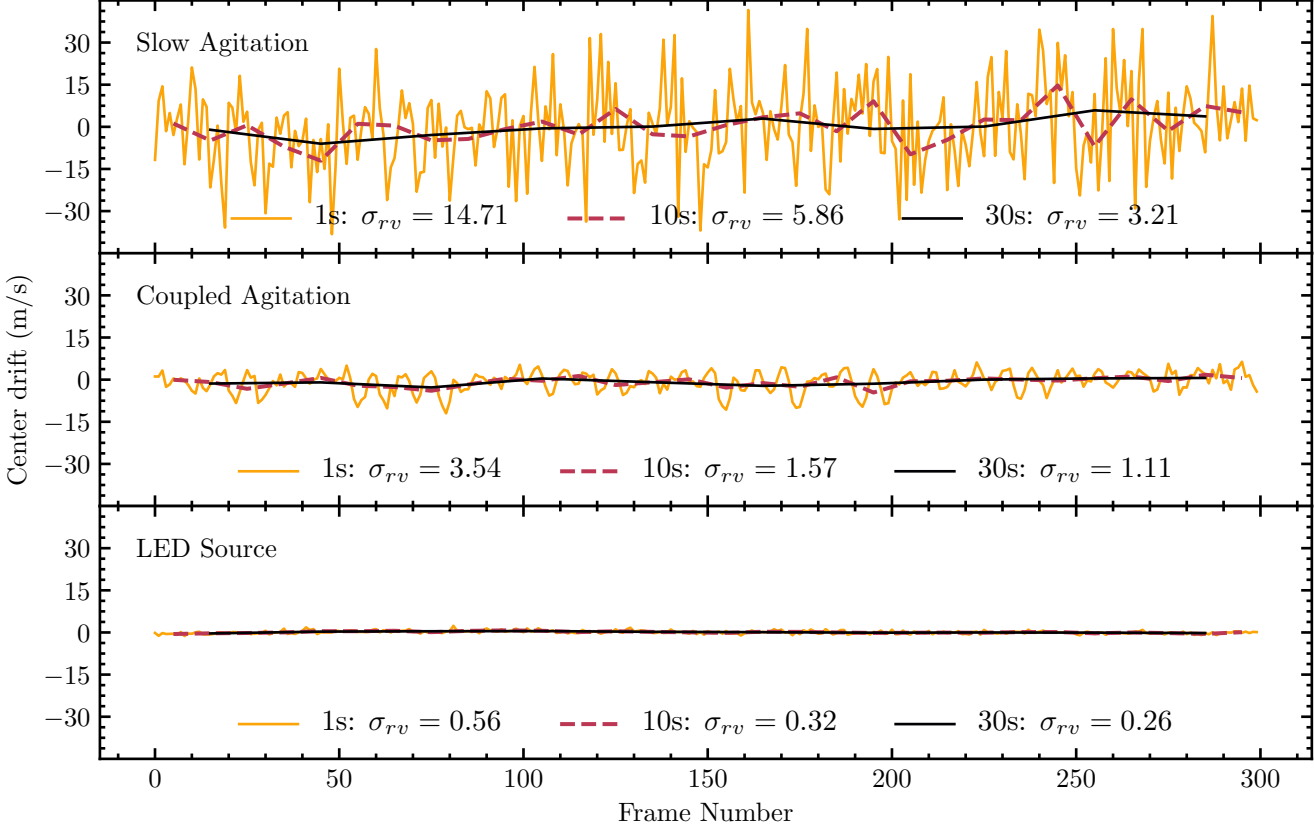


FIG. 11.— Centroid drift and resultant RV error for a slowly agitated fiber (top), coupled agitated fiber (middle), and LED illumination (bottom). The red line in each image is the 30-image average of these centroid drifts, effectively yielding the RV error for 30 second exposures.

means that a large range of fiber configurations are reached after about 10s. We compare this idealized method to a broadband light source (low modal noise) and a slowly agitated fiber (high modal noise). For the slow agitation test, we set only the linear agitator at 80 mm and 0.03 Hz meant to mimic the slight motions of the telescope throughout a night.

The results for these tests are shown in figure 11 where the RV error is calculated using equation 6. The dispersion direction for a rectangular fiber is along the short end, meaning that the diameter  $D$  is 100  $\mu\text{m}$ . The resolution of EXPRES is 150,000 for a 33  $\mu\text{m} \times$  132  $\mu\text{m}$  rectangular fiber, so we use  $R = 50,000$  in equation 6 since our test fiber is three times as large in the dispersion direction.

These results indicate that coupled agitation reduces errors induced by a slowly moving telescope by about three times and are minimized to about  $1.11 \text{ cm s}^{-1}$ . This error is the RV error per line in the spectrograph, meaning that the total RV error could be reduced to below  $10 \text{ cm s}^{-1}$  with at least 120 lines. EXPRES is using a laser frequency comb with approximately  $20 \text{ GHz}$  line spacing leading to between 200-500 lines per order on the spectrograph. This will reduce the RV error per order to below  $8 \text{ cm s}^{-1}$ .

Using our prototype agitation setup in our lab, we were not able to reach the stability of continuum illumination ( $26 \text{ cm s}^{-1}$ ). However, we are confident that increasing the amplitude of circular motion, increasing

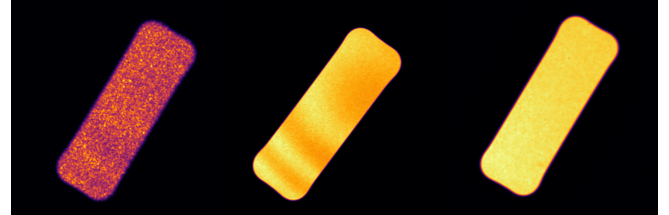


FIG. 12.— Comparison of the long-term agitation methods used in section 5—slow agitation (left), coupled agitation (middle), LED source (right)—as 10s exposures. Brightness directly scales with photon count in these images.

the frequency of both agitators, and adding a “tweeter” element will continue to push this limit even lower.

## 6. SUMMARY AND APPLICATION

We have tested a wide swath of agitation parameter space with the goal of further understanding the mechanism behind fiber agitation as a method for modal noise mitigation. We found that high amplitude, coupled harmonic motion places the fiber into many physical configurations over a short period of time and therefore reduces modal noise extremely efficiently. As shown in figure 12, the coupled agitation method reduces the speckle pattern to levels about as good as a fiber propagating a broadband light source. Such modal noise mitigation can be done at integration times on the order of seconds for relatively dim light source, allowing for direct application to precision RV spectrographs.



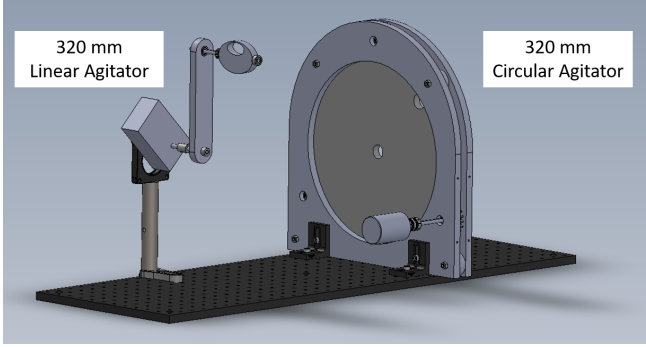


FIG. 13.— Rendering of the proposed fiber agitator for EXPRES. Both the linear and circular agitator have an independent dc motor operated by remote computer control. This agitator will sit on a shelf across the room from the spectrograph and will agitate all fibers that enter the spectrograph during stellar and calibration exposures.

As part of the EXPRES fiber architecture, we will be employing the idealized agitation technique detailed in this paper. We will be combining a 160 mm amplitude circular and linear agitator similar to those seen in figure 2, but with greater stability to support an entire reinforced wrap of cables. A rendering of this design is shown in figure 13. The two agitators will oscillate

at slightly different frequencies at the maximum speed deemed safe for the fibers. We will potentially include a large tweeter attached directly to the cables to add simultaneous high frequency vibrations to the fibers, since it does show marginal improvement to the SNR. This device will agitate all of the fibers that immediately enter the spectrograph, which includes, most importantly, the rectangular science fiber.

We recommend that other precision RV spectrographs consider the results found in this paper when designing their own fiber agitators. Since it only affects the fibers between light sources and the spectrograph, such improved agitation methods can even be added to spectrographs currently taking data to improve SNR and reduce potential false positions. Modal noise is not a problem that should be treated lightly, and its mitigation will help usher in the next-generation of RV spectroscopy and aid in the search for Earth-like worlds.

The Fiber Characterization Station was built with support from the Fund for Astrophysical Research, Inc. Special thanks to Saki Kamon, Kristoffer Acuña, and Dominic Eggerman for their data-taking contributions to this project.



#### REFERENCES

- Baudrand, J., & Walker, G. A. H. 2001, Publications of the Astronomical Society of the Pacific, 113, 851 2, 3
- Chazelas, B., Pepe, F., Wildi, F., et al. 2010, in Proc. SPIE, ed. E. Atad-Ettedgui & D. Lemke, Vol. 7739, 47 1–9 1
- Crepp, J. R., Crass, J., King, D., et al. 2016, in Proc. SPIE, ed. C. J. Evans, L. Simard, & H. Takami, Vol. 9908, 19 1–13 1
- Daino, B., De Marchis, G., & Piazzolla, S. 1980, Optica Acta: International Journal of Optics, 27, 1151 3
- Epworth, R. 1978, in Fourth European Conference on Optical Communication (Genoa: Proceedings of the Fourth E.C.O.C., Genoa), 492–501 2
- Fischer, D., Anglada-Escude, G., Arriagada, P., et al. 2016, PASP, 45 1
- Halverson, S., Roy, A., Mahadevan, S., et al. 2015a, The Astrophysical Journal, 806, 1 1
- Halverson, S., Roy, A., Mahadevan, S., & Schwab, C. 2015b, ApJ Letters, arXiv:1511.02856 1
- Halverson, S., Mahadevan, S., Ramsey, L., et al. 2014, in Proc. SPIE, ed. S. K. Ramsay, I. S. McLean, & H. Takami, Vol. 9147, 1–6 3, 6
- Hunter, T., & Ramsey, L. 1992, Publications of the Astronomical Society of the Pacific, 104, 1244 1
- Imai, M., & Asakura, T. 1979, Optics Communications, 30, 299 2
- Jurgenson, C., Fischer, D., Mccracken, T., et al. 2016, in Proc. SPIE, Vol. 9908 1
- Lemke, U., Corbett, J., Allington-Smith, J., & Murray, G. 2010, in Proc. SPIE, ed. E. Atad-Ettedgui & D. Lemke, Vol. 7739, 24 1–13 2
- Lemke, U., Corbett, J., Allington-Smith, J., & Murray, G. 2011, Monthly Notices of the Royal Astronomical Society, 417, 689 2, 3
- Mahadevan, S., Halverson, S., Ramsey, L., & Venditti, N. 2014, The Astrophysical Journal, 786, 1 2, 3, 6
- McCoy, K. S., Ramsey, L., Mahadevan, S., Halverson, S., & Redman, S. L. 2012, in Proc. SPIE, ed. I. S. McLean & S. K. Ramsay, Vol. 8446, 8J 1–8 3
- Mégevand, D., Zerbi, F. M., Cabral, A., et al. 2012, in Proc. SPIE, ed. I. S. McLean & S. K. Ramsay, Vol. 8446, 1R 1–15 1
- Nikitin, P. V., Stancil, D. D., & Erosheva, E. A. 2011, in IEEE Antennas and Propagation Society, AP-S International Symposium (Digest), Vol. 2, 1662–1665 2
- Plavchan, P. P., Bottom, M., Gao, P., et al. 2013, in Proc. SPIE, ed. S. Shaklan, Vol. 8864, 0G 1–18 1, 3, 5
- Probst, R. A., Lo Curto, G., Avila, G., et al. 2014, in Proc. SPIE, ed. S. K. Ramsay, I. S. McLean, & H. Takami, Vol. 9147, 1C 1–12 1
- Redding, B., Popoff, S. M., & Cao, H. 2013, Optics Express, 21, 6584 2
- Roy, A., Halverson, S., Mahadevan, S., & Ramsey, L. W. 2014, in Proc. SPIE, ed. S. K. Ramsay, I. S. McLean, & H. Takami, Vol. 9147, 1–7 3
- Sablowski, D. P., Plüsckie, D., Weber, M., Strassmeier, K. G., & Järvinen, A. 2015, Astron. Nachr., 1, 0 2, 3
- Spronck, J. F. P., Fischer, D. A., Kaplan, Z., et al. 2015, Publications of the Astronomical Society of the Pacific, 127, 1027 1
- Spronck, J. F. P., Fischer, D. a., & Kaplan, Z. a. 2012, in Recent Progress in Optical Fiber Research, ed. M. Yasin, S. W. Harun, & H. Arof (InTech), 353–370 1
- Stürmer, J., Schwab, C., Grimm, S., et al. 2016, in Proc. SPIE, ed. R. Navarro, Vol. 9912, 1T 1–7 2